Clonk induced response from synchronizer engagements in dual clutch transmissions

Paul D WALKER** and Nong ZHANG**
**Faculty of Engineering and IT, University of Technology, Sydney
PO Box 123, Broadway, NSW 2007, Australia
E-mail: Paul.Walker@uts.edu.au

Abstract
The dual clutch transmission (DCT) is capable of providing mechanical efficiencies comparable to manual transmissions with clutch-to-clutch shifting capabilities of planetary automatic transmissions. Vehicle powertrain equipped with DCTs are considered to be lightly damped dynamic systems, with damping sourced from torsional vibration absorbers and parasitic losses in clutches, transmission and differential considerably less that the damping provided by torque converters in planetary automatics. Consequently, DCTs are exposed to increased response under transient conditions, typically requiring more stringent control strategies for performing clutch-to-clutch shifts, for example. Synchronizer actuation, however, is not given the same detailed level of control to ensure minimization of observable transient response, nevertheless, the high degree of nonlinearity in the mechanisms' actuation presents potential for initiation of undesirable transients. This paper is tasked with investigating the nonlinear engagement of synchronizers contribution to the introduction of noise, vibration, and harshness (NVH). Of particular interest is the initiation of clonk response in the powertrain, considered to be high frequency (300-5000Hz) elasto-acoustic response in powertrains, typically induced through the nonlinear response, such as synchronizer engagement, interacting with frequencies in long hollow shafts.

A multi degree of freedom model of a dual clutch transmission equipped powertrain is presented using lumped inertia-stiffness elements, structured to provide the capabilities for synchronizer engagement using mean engine torque and nonlinear synchronizer models. Synchronizer engagements are undertaken for a variety of input pressures in conditions associated with clonk response. Time and frequency domain results for shaft and sleeve responses post-synchronization are used to evaluate the introduction of frequencies consistent with clonk response. The influence of gear mash nonlinearity and chamfer alignment on the synchronizer response is also studied.

Keywords: Dual clutch transmission, Synchronizer, Backlash, Powertrain

1. Introduction

Dual clutch transmissions realize shifting through the actuation of synchronizers to select the shifting gear before clutch-to-clutch shifting can be initiated. Thus synchronizer engagement is a precursor to gearshift and must therefore contribute to delay in the engagement process once a requirement to shift is detected. As an example Rolland (1) suggests that the engagement may be in the region of 100-200ms. Socin & Walters (2) provide a detailed background into the modeling of synchronizer mechanisms, and along with Lechner & Naunheimer (3), the complex nature of engagement and appreciation of the

delay present in a synchronizers actuation can be identified. Limitations of component size, particularly for the cone clutch and indexing chamfers, impact on the ability to minimize the duration of engagement. However, the externally applied load, typically through hydraulic control valves, can be manipulated easily to reduce engagement through increased torque generated in the cone clutch and dog gear.

Research in Galvagno (4) presents several simple models for simulating the engagement of synchronizers using few degrees of freedom, investigating only the speed matching in the synchronizer, making use of a simplified mechanism model. Numerical simulations of synchronizer actuation conducted by Hoshino (5) and Liu (6) demonstrate the nonlinear nature of synchronizer engagement, and the detail required in modeling its actuation, considering both cone clutch and indexing torques.

One particular limitation to automation of synchronizer engagements in the DCT is the initiation of audible response in the powertrain, known as *clonk*. Here frequency excitations of shafts in regions near it main breathing modes will result in such an outcome[7], particularly for frequencies in the range of 300 to 5000 Hz[7]. Such responses are frequently identified as being initiated through nonlinear events in the powertrain, such as gear backlash[7] or engine valve[8]. To investigate such phenomena detailed powertrain models are developed for simulating the frequency resulting from nonlinear events.

The remainder of this paper is allocated to presentation of (i) a lumped mass model of a simplified DCT powertrain including engine, synchronizer, and vehicle resistance torque models, (ii) damped free vibration analysis of the powertrain to identify natural frequencies of the system for comparison to transient data, (iii) simulation of synchronizer engagements under a range of hydraulic pressures and chamfer alignments, and (iv) introduction of gear and synchronizer mesh nonlinearities to the model for study of transient response. Finally, (v) the paper is summarized and conclusions are drawn.

2. Powertrain modeling

Vehicle powertrain modeling using lumped inertias has been performed using torsional methods for a semi-definite system, as set out in Rao (9). Elements of the powertrain, shown in Figure 1, comprise of engine, flywheel, clutch drum, transmission, including clutch plates, gear pairs and synchronizers, final drive ratio, propeller shaft, differential, wheel hub and vehicle inertias. Specifically for synchronizer engagement, clutch 1 is engaged with the drum, and synchronizer 1 is closed, with synchronizer 2 and clutch 2 open. Thus the engine drives the vehicle through the first gearset and the second gearset is synchronized for shifting.

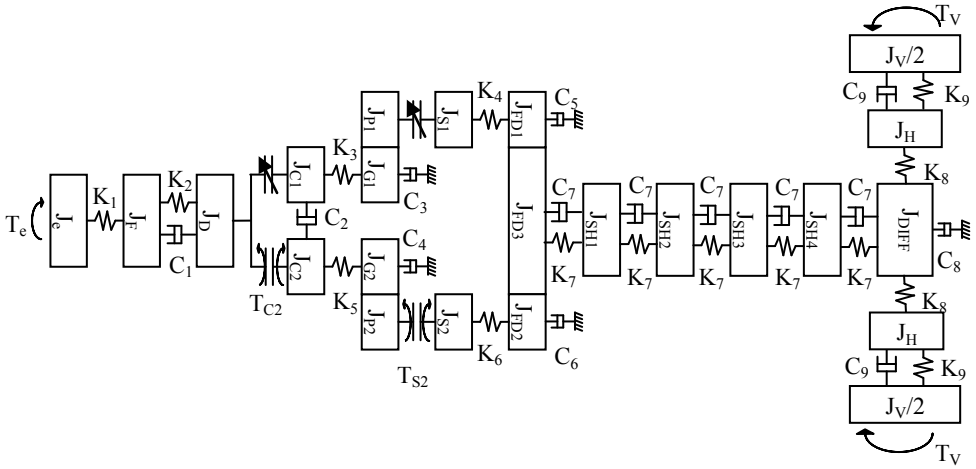

Fig. 1: DCT powertrain lumped inertia model

In conjunction with the powertrain model, the equations of motion are:

$$J_e\ddot{\theta}_e - K_1(\theta_F - \theta_e) = T_e \tag{1}$$

$$J_F\ddot{\theta}_F + K_1(\theta_F - \theta_e) - K_2(\theta_D - \theta_F) - C_1(\dot{\theta}_D - \dot{\theta}_F) = 0 \tag{2}$$

$$(J_D + J_{C1})\ddot{\theta}_D + K_2(\theta_D - \theta_F) + C_1(\dot{\theta}_D - \dot{\theta}_F) - K_3(\theta_{G1} - \theta_D) - C_2(\dot{\theta}_{C2} - \dot{\theta}_D) = -(T_{C2}) \tag{3}$$

$$J_{G1}\ddot{\theta}_{G1} + K_3(\theta_{G1} - \theta_D) - C_3\dot{\theta}_{G1} - r_{G1}K_T(\theta_{G1}r_{G1} + x_1 - \theta_{P1}r_{P1} - y_1) = 0 \tag{5}$$

$$J_{P1}\ddot{\theta}_{P1} + r_{P1}K_T(\theta_{G1}r_{G1} + x_1 - \theta_{P1}r_{P1} - y_1) - r_{S1}K_S(\theta_{P1}r_{S1} - \theta_{S1}r_{S1}) = 0 \tag{6}$$

$$J_{S1}\ddot{\theta}_{S1} - K_4(\gamma_{FD1}\theta_{FD3} - \theta_{S1}) + r_{S1}K_S(\theta_{P1}r_{S1} - \theta_{S1}r_{S1}) = 0 \tag{7}$$

$$J_{C2}\ddot{\theta}_{C2} - K_5(\theta_{G2} - \theta_{C2}) - C_2(\dot{\theta}_{C1} - \dot{\theta}_{C2}) = T_{C2} \tag{8}$$

$$J_{G2}\ddot{\theta}_{G2} + K_5(\theta_{G2} - \theta_{C2}) - C_4\dot{\theta}_{G2} - r_{G2}K_T(\theta_{G2}r_{G2} + x_2 - \theta_{P2}r_{P2} - y_2) = 0 \tag{9}$$

$$J_{P2}\ddot{\theta}_{P2} + r_{P2}K_T(\theta_{G2}r_{G2} + x_2 - \theta_{P2}r_{P2} - y_2) = -T_{S2} \tag{10}$$

$$J_{S2}\ddot{\theta}_{S2} - K_6(\gamma_{FD2}\theta_{FD3} - \theta_{S2}) = T_{S2} \tag{11}$$

$$\begin{aligned}&(\gamma_1^{\,2}\cdot J_{FD1} + \gamma_2^{\,2}\cdot J_{FD2} + J_{FD3})\ddot{\theta}_{FD3} + \gamma_{FD1}K_4(\gamma_{FD1}\cdot\theta_{FD1} - \theta_{S1}) + \gamma_{FD2}K_6(\gamma_{FD2}\cdot\theta_{FD2} - \theta_{S2})\\ &- K_7(\theta_{SH1} - \theta_{FD3}) - (\gamma_{FD1}C_5 + \gamma_{FD2}C_6)\dot{\theta}_{FD3} - C_7(\dot{\theta}_{SH1} - \dot{\theta}_{FD3}) = 0\end{aligned} \tag{12}$$

$$J_{SH1}\ddot{\theta}_{SH1} + K_7(\theta_{SH1} - \theta_{FD3}) - K_7(\theta_{SH2} - \theta_{SH1}) + C_7(\dot{\theta}_{SH1} - \dot{\theta}_{FD3}) - C_7(\dot{\theta}_{SH2} - \dot{\theta}_{SH1}) = 0 \tag{13}$$

$$J_{SH2}\ddot{\theta}_{SH2} + K_7(\theta_{SH2} - \theta_{SH1}) - K_7(\theta_{SH3} - \theta_{SH2}) + C_7(\dot{\theta}_{SH2} - \dot{\theta}_{SH1}) - C_Y(\dot{\theta}_{SH3} - \dot{\theta}_{SH2}) = 0 \tag{14}$$

$$J_{SH3}\ddot{\theta}_{SH3} + K_7(\theta_{SH3} - \theta_{SH2}) - K_7(\theta_{SH4} - \theta_{SH3}) + C_7(\dot{\theta}_{SH3} - \dot{\theta}_{SH2}) - C_7(\dot{\theta}_{SH4} - \dot{\theta}_{SH3}) = 0 \tag{15}$$

$$J_{SH4}\ddot{\theta}_{SH4} + K_7(\theta_{SH4} - \theta_{SH3}) - K_7(\theta_{DIFF} - \theta_{SH4}) + C_7(\dot{\theta}_{SH4} - \dot{\theta}_{SH3}) - C_7(\dot{\theta}_{DIFF} - \dot{\theta}_{SH4}) = 0 \tag{16}$$

$$J_{DIFF}\ddot{\theta}_{DIFF} + K_7(\theta_{DIFF} - \theta_{SH4}) - 2K_8(\theta_T - \theta_{DIFF}) + C_7(\dot{\theta}_{DIFF} - \dot{\theta}_{SH4}) - C_8\dot{\theta}_{DIFF} = 0 \tag{17}$$

$$2J_H\ddot{\theta}_H + 2K_8(\theta_H - \theta_{DIFF}) - 2K_9(\theta_T - \theta_H) - 2C_9(\dot{\theta}_T - \dot{\theta}_H) = 0 \tag{18}$$

$$2J_V\ddot{\theta}_T + 2K_9(\theta_T - \theta_H) + 2C_9(\dot{\theta}_T - \dot{\theta}_H) = -T_V \tag{19}$$

$$M_G\ddot{x}_1 - K_{B1}x_1 - C_{B1}\dot{x}_1 - K_T(\theta_{G1}r_{G1} + x_1 - \theta_{P1}r_{P1} - y_1) = 0 \tag{20}$$

$$M_P\ddot{y}_1 - K_{B1}y_1 - C_{B1}\dot{y}_1 + K_T(\theta_{G1}r_{G1} + x_1 - \theta_{P1}r_{P1} - y_1) = 0 \tag{21}$$

$$M_G\ddot{x}_2 - K_{B2}x_2 - C_{B2}\dot{x}_2 - K_T(\theta_{G2}r_{G2} + x_2 - \theta_{P2}r_{P2} - y_2) = 0 \tag{22}$$

$$M_P\ddot{y}_2 - K_{B2}y_2 - C_{B2}\dot{y}_2 + K_T(\theta_{G2}r_{G2} + x_2 - \theta_{P2}r_{P2} - y_1) = 0 \tag{23}$$

Backlash is modeled using a piecewise stiffness element, where if the contact is below a specified region there is no contact between meshing parts, and therefore no contact stiffness.

$$K_T = \begin{cases} 0 & |\theta_G r_G + x - \theta_P r_P - y| < x_C/2 \\ 10^8 & |\theta_G r_G + x - \theta_P r_P - y| \geq x_C/2 \end{cases} \tag{24}$$

$$K_S = \begin{cases} 0 & |\theta_P - \theta_S| < \theta_C/2 \\ 10^8 & |\theta_P - \theta_S| \geq \theta_C/2 \end{cases} \tag{25}$$

To reduce degrees of freedom in the model it is assumed that there is no backlash in gears or engaged synchronizers and that wheels are symmetrical and can be lumped together. Equations 5-7 and 9-10 are replaced with the following equations of motion and bearing translational degrees of freedom are eliminated, as a result the degrees of freedom are reduced from 23 to 14.

$$\left(J_{G1} + \left(J_{P1} + J_{S1}\right)/\gamma_1^{\,2}\right)\ddot{\theta}_{G1} + K_3\left(\theta_{G1} - \theta_{C1}\right) - C_3\dot{\theta}_{G1} - \frac{K_4}{\gamma_1}\left(\gamma_{FD1}\theta_{FD3} - \frac{\theta_{S1}}{\gamma_1}\right) = 0 \tag{26}$$

$$\left(J_{P2}/\gamma_2^{\,2} + J_{G2}\right)\ddot{\theta}_{G2} + K_5\left(\theta_{G2} - \theta_{C2}\right) - C_4\dot{\theta}_{G2} = -T_{S2}/\gamma_2 \tag{27}$$

$$J_{S2}\ddot{\theta}_{S2} - K_6\left(\gamma_{FD2}\theta_{FD3} - \theta_{S2}\right) = T_{S2} \tag{28}$$

Synchronizer model is adopted from Walker (10) where cone, blocking and indexing torques are modeled, with the sleeve model coupling hydraulic control system to engage then mechanism. The synchronizer hydraulic actuation system comprises of high flow on/off solenoids actuating a double acting piston arrangement, applying engagement load to the mechanism. Cone clutch and indexing torque must be considered in a piecewise manner depending on the manner of engagement and load on the mechanism. The cone torque is adopted from Paffoni (11) for first free fly, with oil wiping, and dry friction, with the inclusion of a lock up rationale.

$$T_C = \begin{cases} 4\pi\mu R_m^3 b\dfrac{\dot{\theta}_{syn}}{h} & X_S < 2 \\ \dfrac{\mu_C F_S R_C}{\sin\alpha} & X_S \geq 2, \dot{\theta} \neq 0 \\ T_{SYN} & X_S \geq 2, \dot{\theta} = 0 \\ \dfrac{\mu_{C,S} F_S R_C}{\sin\alpha} & X_S \geq 2, \dot{\theta} = 0, T_D > T_C \end{cases} \tag{29}$$

Here T_{SYN} is the average synchronizer torque, in the similar reference frame to drag torque, and is derived from equation (25) thus:

$$T_{SYN} = -\gamma_2\left[\left(J_{P2}/\gamma_2^{\,2} + J_{G2}\right)\ddot{\theta}_{G2} + K_5\left(\theta_{G2} - \theta_{C2}\right) - C_4\dot{\theta}_{G2}\right] \tag{30}$$

This equation is maintained through the speed synchronization and ring unblocking steps of engagement according to Walker (10). However, during the remaining stages the applied load (F_S) is considered as a function of net torque on the mechanism and sliding friction of the sleeve over the ring, thence:

$$T_C = \mu_R R_I T_D \times \frac{\mu_{C,S} R_C}{\sin\alpha} \tag{31}$$

The blocking, or indexing, torque is dependent on the direction of sleeve velocity ($\dot{x}$) and side of chamfer engagement (λ). Indexing torque is represented as:

$$T_I = \begin{cases} FR_I \dfrac{1-\mu_I \tan\beta}{\mu_I + \tan\beta} & \lambda + ve, \dot{x} + ve \\ FR_I \dfrac{1+\mu_I \tan\beta}{\mu_I - \tan\beta} & \lambda + ve, \dot{x} - ve \\ -FR_I \dfrac{1+\mu_I \tan\beta}{\mu_I - \tan\beta} & \lambda - ve, \dot{x} + ve \\ -FR_I \dfrac{1-\mu_I \tan\beta}{\mu_I + \tan\beta} & \lambda - ve, \dot{x} - ve \end{cases} \quad (32)$$

Engine torque is modeled using a steady state engine map, with torque a function of speed and throttle. Vehicle torque model is derived from three resistance forces of aerodynamic drag, rolling resistance, and incline load. These are equated to torques by multiplying by the wheel radius, as shown in the equation below.

$$T_V = \left(M_v g \sin(\varphi) + \frac{1}{2} \rho_{air} A_v C_D V^2 + M_v g C_T \right) \times R_W \quad (33)$$

3. Damped free vibration analysis

Free vibration analysis is used here to compare powertrain models with and without backlash. To model backlash all lash zones are assumed to be in contact and the synchronizer is considered to be engaged. Damped free vibration analysis is applied to both models, with natural frequencies and damping ratios presented for both models. Modal shapes are then used to identify relationship of natural frequency to the model.

Table 1: Damped free vibration results of powertrain with and without backlash

	No Backlash Model		Backlash Model	
Frequency number	Natural frequency (Hz)	Damping ratio (%)	Natural frequency (Hz)	Damping ratio (%)
RBM	0	-	0	0
1	5.5	0.19	5.1	0.17
2	34.2	1.29	32.1	1.32
3	97.7	0.06	61.7	0.28
4	225.2	0.44	100.4	0.07
5	231	0.19	122.7	0.08
6	325.4	0.16	225.1	0
7	736.6	0.01	225.1	0
8	1274.1	0.02	230.9	0.09
9	1568.5	0.74	236.3	0.61
10	1926.1	0.01	563.1	0.02
11	2969.5	1.41	768.4	0
12	4084.9	1.95	939.8	0.01
13	4801.2	2.29	1564	1
14	-	-	1698.2	0
15	-	-	1947	0.01
16	-	-	2114.5	0.01
17	-	-	2885.4	0
18	-	-	2969.7	1.78
19	-	-	3427.7	0
20	-	-	4084.8	2.21

Damped free vibration results provide two important characteristics of the powertrain. First, damping ratio results demonstrate that lightly damped nature of the powertrain, where no damping ratio exceeds 10%. Second, through the introduction of nonlinear mesh contacts in the powertrain several more frequencies are introduced in the range associated with clonk excitation. This provides more sources of excitation in the powertrain resulting from nonlinearities that can contribute to the initiation high frequency vibration in the propeller shaft.

4. Synchronizer engagement simulations

Simulations of synchronizer engagement are conducted using the original model for the powertrain, assuming the no backlash condition in gears and synchronizers. Simulations are conducted in Matlab using ODE45 with a maximum time step of 10^{-6}, and relative and absolute tolerances set to 10^{-4} and 10^{-7}, respectively. The initial vehicle speed is 40 rad/s and engine speed 182 rad/s. Maximum control line pressures are 1-5 and 10MPa.

4.1 Transient simulations without backlash

Simulations of synchronizer engagement are conducted using the original model for the powertrain, assuming the no backlash condition in gears and synchronizers. Simulations are conducted in Matlab using ODE45 with a maximum time step of 10^{-6}, and relative and absolute tolerances set to 10^{-4} and 10^{-7}, respectively. The initial vehicle speed is 40 rad/s and approximate engine speed of 182 rad/s. Maximum control line pressures are 1-5 and 10MPa.

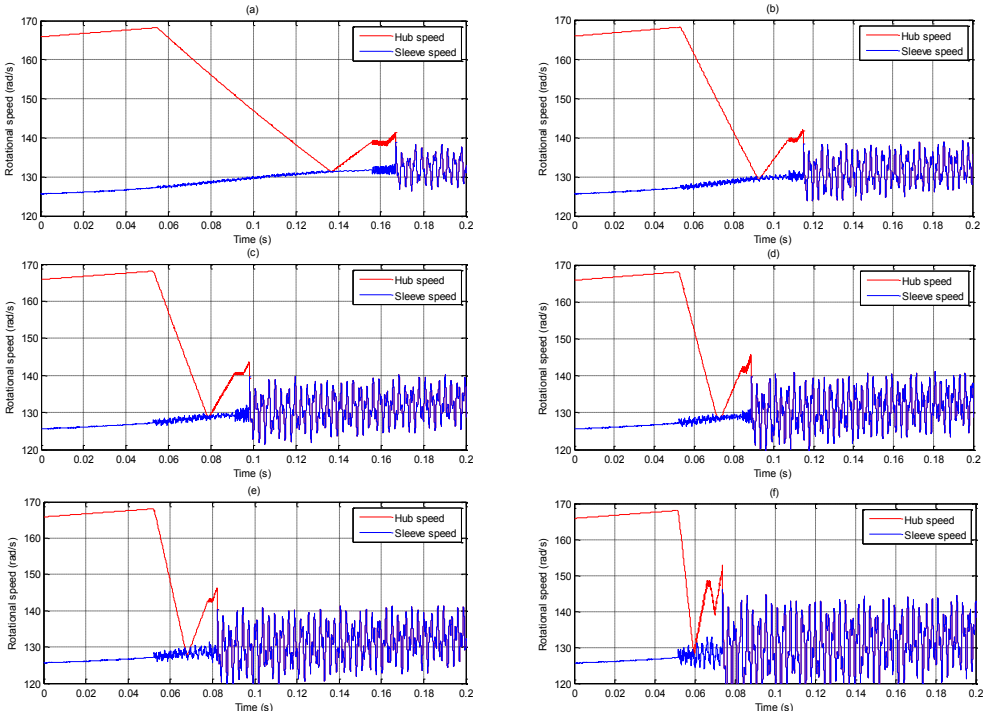

Fig. 2: Synchronizer engagement results of sleeve and hub speeds at different input pressures. (a) 1MPa, (b) 2MPa, (c) 3MPa, (d) 4MPa, (e) 5MPa, and (f) 10MPa

The results in Fig. 2 (a) show how synchronizer engagement occurs in the transmission. It shows the initial steady state speed of the synchronizer and gear to be above that of sleeve. This is a consequence of high wet clutch drag torque, such that before synchronization commences the losses in the wet clutch are minimized by reducing the slipping speed in the clutch. Thus, maximum wet clutch drag must be reached as

synchronization completes at 0.14s. Between 0.14 and 0.16s unblocking of the synchronizer ring occurs. At completion of this process, there exists a relative speed between gear and sleeve, and by releasing the cone clutch at the end of ring unblocking the relative speed cannot be recovered. This shortens the duration of indexing as there is already relative motion between sleeve and gear as the engagement of the dog gears occurs. However this relative speed at the completion of indexing is also produces an impulsive torque as the sleeve traps the gear, initiating response at completion of engagement.

Simulation results in Fig. 2 demonstrate the influence of input line pressure on the speed of synchronization. In (a), at the lowest control pressure, the engagement takes over 120ms, in (b) with pressure 2MPa engagement takes approximately 60ms, however as line increases through to 10MPa the engagement takes 20ms, indicating that the result is not directly proportional to the duration of engagement, as would be indicated by equations (27) – (30). The results also demonstrate the resulting response of the sleeve as the sleeve and gear hub splines mesh to complete lockup. It shows that the realignment of chamfers increases relative speed before the gear hub is trapped by the sleeve, and the resulting abrupt change in gear hub speed excites vibration in the sleeve through an impulse generated as the gear hub matches speed with the sleeve upon the completion of indexing.

The limitation to these simulation results is that the impulse is calculated numerically, and is therefore dependent on the step time of the solver; it is therefore possible to overestimate the maximum impulse generated. However as the peak speed of the hub immediately before the completion of engagement increases substantially from fig. 2 (a) to (f) the impulse generated must also increase significantly. Thus it is demonstrated that the line pressure will contribute significantly to the post engagement response of the synchronizer sleeve.

3.2 Transient simulations with backlash

Similar simulations with the inclusion of backlash in the powertrain model are conducted for 1, 2, 5 and 10 MPa line pressures. The same initial conditions are used here as previous simulations, however maximum time step is set to 10^{-7}.

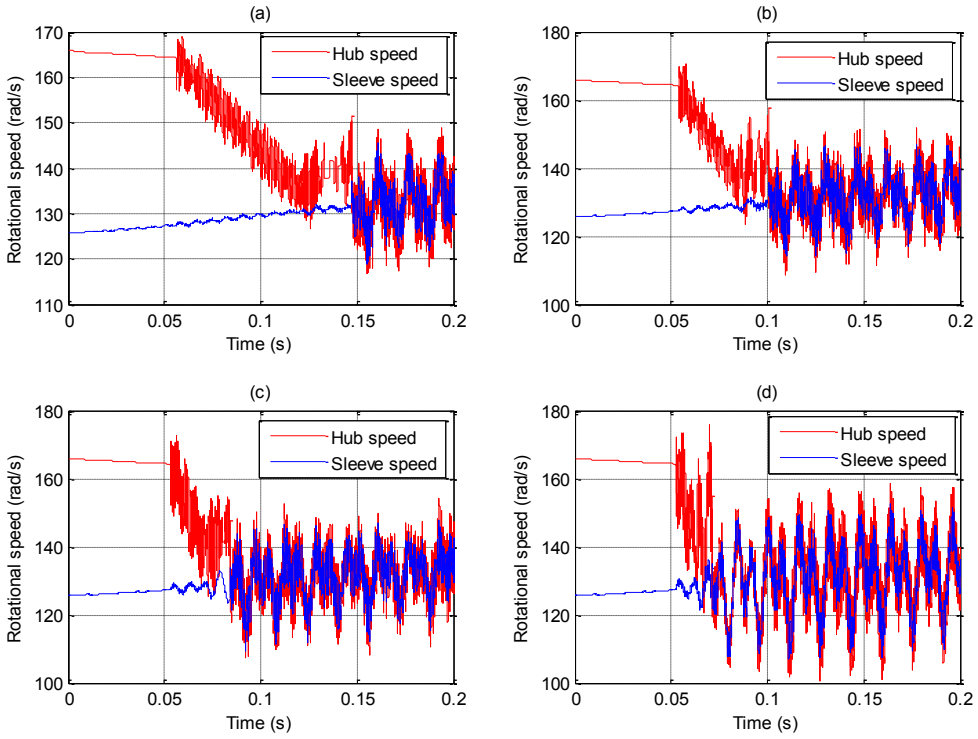

Fig. 3: Synchronizer engagement results of sleeve and hub speeds at different input pressures. (a) 1MPa, (b) 2MPa, (c) 5MPa, and (d) 10MPa

The results shown in Fig. 3 are reasonably consistent with those in Fig. 2, where increase of synchronizer control pressure reduces the synchronizer engagement, but introduces further issues in excitation of the sleeve, particularly after the process of engagement is completed. The backlash present between both gear and pinion and pinion and synchronizer sleeve produces considerable higher frequency vibrations in the mesh contact, these results from abrupt engagement of the synchronizer cone clutch. Again, the results shown that increasing the control pressure exacerbates the sleeve response after the synchronizer is engaged.

There are two limitations to these simulations. First, the mesh contacts are modeled without damping. Second, the impulse resulting from synchronizer lockup is determined numerically, and the peak torque impulse may therefore be overestimated. Through these two limitations the peak vibration amplitudes are likely to be overestimated, limiting these results.

5. Propeller shaft frequency responses

The simplest strategy for reducing the engagement time for synchronizers is to increase the control line pressure. However, nonlinear response of the system suggests that this can increase the likelihood of initiating audible clonk response in the powertrain. In this section the post engagement frequency response in propeller shaft elements is evaluated using Fast Fourier Transforms to identify frequencies excited as a result of synchronizer engagement, and which of these frequencies are dominant at different control pressures.

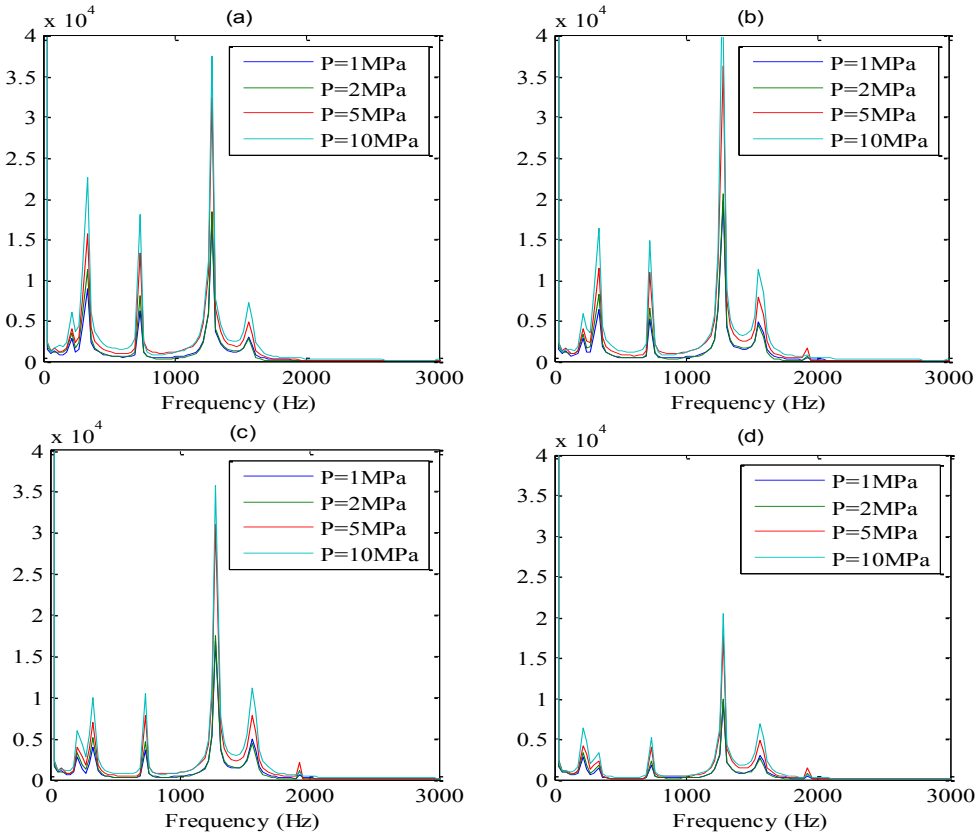

Fig. 4: Frequency domain results of propeller shaft element speeds after synchronization without backlash model (a) element 1, (b) element 2, (c) element 3, and (d) element 4

Frequency domain results in Fig. 4 (a) to (d) show that the response present in the propeller shaft as a result of synchronizer engagement is dominated by frequencies in the

region of 200 to 2000Hz. Resulting from the increase in lime pressure there is significant increase in the amplitude of responses. Above 5MPa for results in (b)-(d) a frequency at 2000Hz is excited in the shafts. This indicates that the increase in pressure exacerbates the propeller shaft frequency response. The results shown that while it is possible to generate frequency responses in the propeller shaft these frequencies are not broad spectrum, and do not cover the range of available natural frequencies shown in Table 1.

The Fast Fourier Transform results for the nonlinear backlash model are shown in Fig. 5. These results indicate the presence of more frequencies in the shaft in the region between 1000 and 3000Hz. This is a more clear indication that the use of backlash models in the simulation contribute to further excitation of the propeller shaft elements, and is more representative of the frequency results that would be expected for clonk response resulting from synchronizer engagement. This suggests that the gear backlash has a more significant role in exciting the propeller shaft than the nonlinear nature of synchronizer engagement alone. Furthermore higher pressures for synchronizer engagement increase the frequency response significantly, particularly in the region of 3000Hz. These results suggest that the higher engagement pressures contribute to the excitation of powertrain frequencies that are in a range that can be reasonable expected to initiate clonk response.

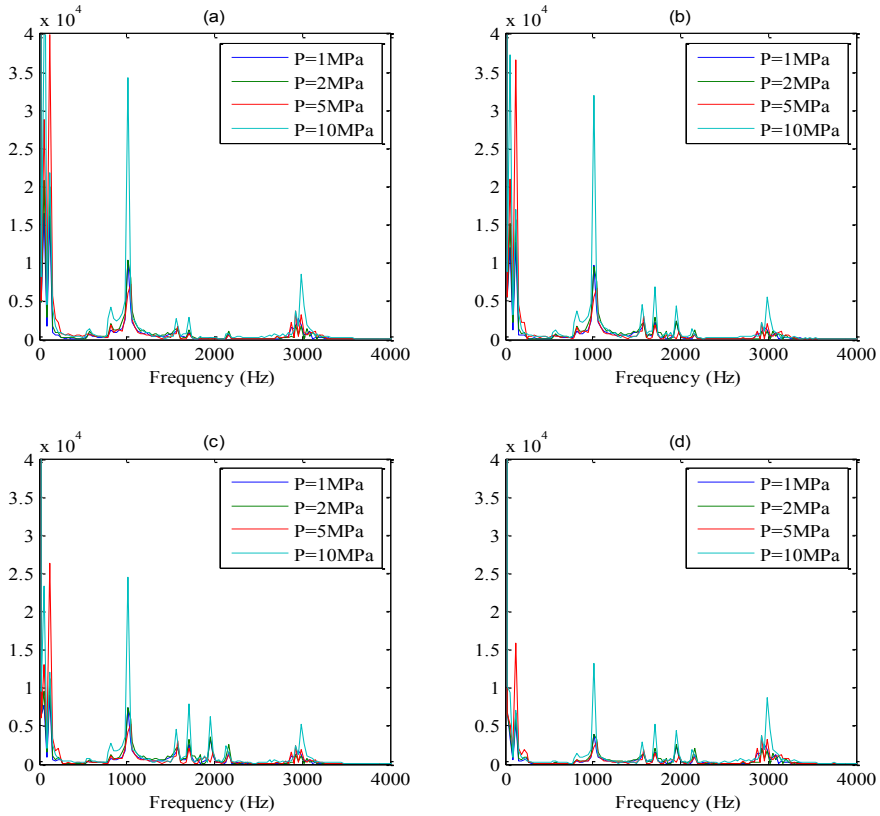

Fig. 5: Frequency domain results of propeller shaft element speeds after synchronization with backlash model (a) element 1, (b) element 2, (c) element 3, and (d) element 4

6. Conclusions

This paper has presented to model variants for investigating synchronizer engagements in dual clutch transmissions. The focus of this investigation has been the evaluation of the influence of synchronizer control pressure on synchronizer actuation and the response of the powertrain after engagement is completed. Particular emphasis has been placed on the frequency domain response in the propeller shafts after engagement is complete, and the influence that this may have on the excitation of frequencies consistent with clonk type response of in the powertrain. This is particularly important as audible responses, such as

those elicited from clonk, are a major limiting factor to the use of high pressure to reduce the duration of synchronizer engagement in DCTs.

To perform this investigation, models of a powertrain were developed using both constant gear mesh, and gear and synchronizer mesh with backlash. The inclusion of additional degrees of freedom with backlash models increases the system natural frequencies, particularly in the range of 400-4000H, as shown in the free vibration analysis section. Transient simulations were conducted using a range of synchronizer control pressures with both model variants. The results indicate that nonlinearities present in the synchronizer alone are not sufficient for the model to excite a broad range of natural frequencies. However, the backlash model produced results that indicate a broad range of frequencies between 1000 and 3000Hz are excited during synchronizer engagement. This is particularly evident when the control pressure is increased to 5 and 10MPa, resulting in significant increases to post engagement response of both the sleeve and propeller shaft elements in the model. It should be noted that to demonstrate clonk type excitation of the powertrain experimental verification is required.

References

(1) Socin, R. J. and Walters, L. K., Manual Transmission Synchronizers, SAE Technical Paper 680008, 1968

(2) Lechner, G. and Naunheimer, H., Automotive Transmissions - Fundamentals, Selection, Design and Application, Springer-Verlag, 1999

(3) Rolland, D., O'Neill, A., Burchell, T., et al., Hew High performance Dual clutch transmission, Proceedings of the FISITA World Congress. Paper: F2006P005, 2006

(4) Galvagno, E., Velardocchia, M., and Vigliani, A., Dynamic and kinematic model of a dual clutch transmission, Mechanism and Machine Theory, Volume 46, 2011, pp794-805

(5) Hoshino, H., Analysis on Synchronisation Mechanism of Transmission, SAE Technical paper: 1999-01-0734, 1999

(6) Liu, Y. and Tseng, C., Simulation and Analysis of Synchronisation and Engagement on Manual Transmission Gearbox, Int. J. Vehicle Design, Volume 43(1-4), 2007, pp. 200-220

(7) Theodossiades, S., Gnanakumarr, M., Rahnejat, H. and Menday, M., Mode identification in impact-induced high-frequency vehicular driveline vibrations using an elasto-multi-body dynamics approach, Proceedings of the IMechE, Part K: Journal of Multi-body Dynamics, Volume 218(2), 2004 pp. 81-94.

(8) Teodorescu, M., Theodossiades, S. and Rahnejat, H., Multi-physics approach to design analysis of powertrain sub-systems, 12th IFToMM World Congress, Besancon France, 2007

(9) Rao, S. S., Mechanical Vibrations, Addison-Wesley Publishing Co 1986

(10) Walker, P. D., Zhang, N., Tamba, R. and Fitzgerald, S., Synchroniser modeling with application specific to the dual clutch transmission, 13th APVC, 2009

(11) Paffoni, B., Progri, R., Gras, R. and Blouet, J., The hydrodynamic phase of Gearbox syncrhomesh operation: the influence of radial and circumferential grooves, Proceedings of the IMechE: Part J: J Engineering Tribology, Volume 211, 1997, pp. 107-116.

Acknowledgements

Financial support for this project is provided jointly by the Australian Research Council (Linkage ID number LP0775445) and NTC Powertrains.